SIMULATION OF SEMICONDUCTOR DEVICES AND PROCESSES Vol. 3
Edited by G. Baccarani, M. Rudan - Bologna (Italy) September 26-28, 1988 - Tecnoprint

PHYSICAL PARAMETER EXTRACTION BY INVERSE MODELLING OF SEMICONDUCTOR DEVICES

G.J.L. Ouwerling, F. van Rijs, H.M. Wentinck,
J.C. Staalenburg and W. Crans

Delft University of Technology, Faculty of Electrical Engineering, Electrical Materials Laboratory, Mekelweg 4, P.O. Box 5031, 2600 GA DELFT, the Netherlands.

Abstract: Inverse modelling is the use of minimization procedures combined with forward device models for parameter extraction. Theory and two practical examples are presented.

1. INTRODUCTION

Semiconductor device modelling has reached a level of maturity that allows for extensive application in 'real-world' environments. At this stage, no longer the numerical solution of the model's equations, but the accuracy of the physical parameters used in the model limits the adequacy of a semiconductor device simulation. For conventional macroscopical semiconductor models, the physical parameters describe the doping profile, carrier generation and recombination processes and carrier mobility as a function of the device geometry and the

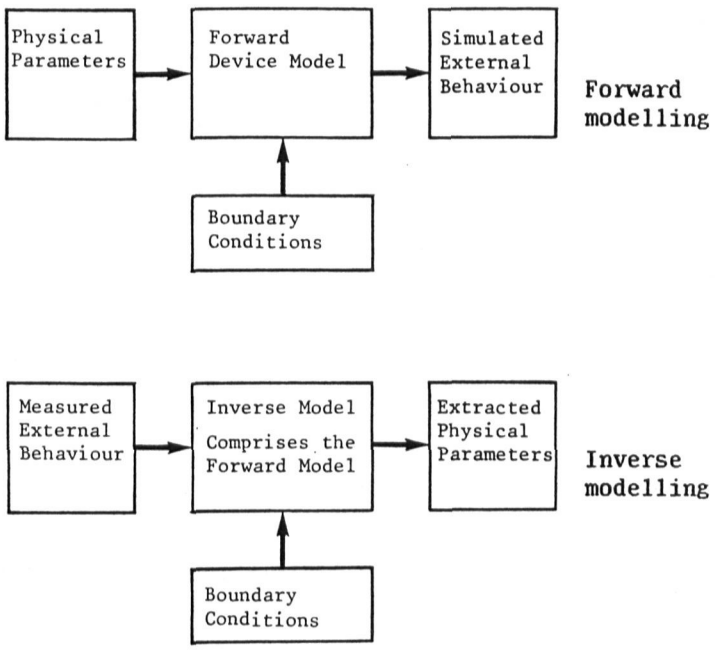

Fig. 1. Relationship between forward and inverse modelling

physical state of the device. It is essential that these parameters are available with values that accurately apply to actual fabrication technologies and in a form compatible with the device simulation package used.

Many methods for the direct measurement of the physical parameters are known. In general, these methods all have certain disadvantages in common. The methods are:

- in general, applicable to one spatial dimension only;
- subject to measurement error due to simplifications in the physical models (e.g. the abrupt depletion approximation);
- applied to dedicated measurement devices that may differ considerably from the devices for which the physical parameters are needed.

To alleviate these disadvantages, the concept of inverse modelling is introduced. Fig. 1 depicts the relationship between forward modelling and inverse modelling. In the case of forward modelling, the external device behaviour is calculated from physical parameters using geometrical device information; in the inverse case, exactly the opposite is done. With an inverse model the external device behaviour (e.g. measured characteristics) is used to determine the physical parameters. Internally, this inverse model employs exactly the same device model that is used for the forward modelling of the class of devices under study.

In general, inverse modelling is implemented by applying the forward model to various sets of physical parameters. Starting from a first "guestimate" of the parameters involved, an iterative computation scheme minimizes the difference between the measured and the modelled device behaviour. This is depicted schematically in fig. 2. The forward device model and the minimization procedure are separate entities in the inverse model; the minimization process is guided by the simulated external device behaviour only. Therefore, it is possible to use an existing forward model (e.g. in the form of a device simulation package) together with an external minimization procedure.

Advantages of parameter extraction by inverse modelling are:

- In situ measurements are a logical consequence of the use of the forward device model;
- Parameters become available in a form precisely fitted for use in the forward model;
- No accuracy limiting assumptions, such as the abrupt depletion approximation, have to be made;
- The parameters can be determined as a function of more than one spatial dimension.

In fact, the accuracy of the parameters found is no longer determined by the measurement interpretation method, but by the accuracy of the forward model used in the inverse modelling

procedure (and evidently by the error on the measurement data). In principle, the use of 2D or 3D models is only a matter of computer time. The same holds for more accurate modelling of charge-carrier transport mechanisms (e.g. by Monte Carlo methods).

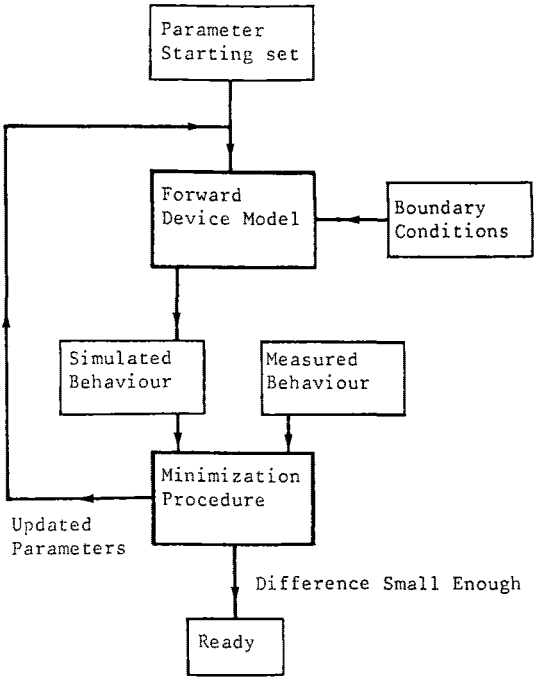

Fig 2. Inverse modelling by minimization techniques

Some risks and disadvantages of inverse modelling must be noted:

- No more information than the forward model can contain can be found. For instance, if the physical model of the carrier mobility in the forward device model does not describe the dependence on the electric field, than this dependence will not be detected by inverse modelling;
- The final solution for the parameters to which the iterative scheme converges is nonunique in the mathematical sense. If too many dependent physical parameters are determined simultaneously, erroneous values may be found. However, minimization schemes are able to detect (but not resolve) such dependencies;
- It may be necessary to evaluate the forward model many times. This can be computationally expensive.

The choice of a suitable minimization method for inverse modelling, and its implementation in the form of a parameter determination driver program is discussed below. We will also illustrate the method of inverse modelling with two applications. The first is the determination of doping profiles from CV measurements; the second the determination of the electric field profile in an amorphous silicon p-i-n structure by time-of-flight measurements.

We remark that identical inverse modelling techniques were succesfully applied in geophysics and led to important breakthroughs in hydrocarbon exploration [1].

2. INVERSE MODELLING BY NONLINEAR MINIMIZATION TECHNIQUES

Minimizing the difference between measured and simulated device behaviour can be effected by minimizing a weighted sum of squared differences, commonly called the least squares error

$$\xi(p) = \sum_i \left[\frac{y_m(i) - y_s(i;p)}{w(i)}\right]^2$$

Here y_m denotes measured and y_s simulated quantities, and p is the vector of all parameters to be determined. The measurements may depend on more than one excitation, for instance on several different voltages applied to the device. The counter i enumerates all measurements that are to be considered. The weight function w(i) controls the contribution of each difference to the error sum. It may serve several purposes:

- to bring different measured quantities in the same value range;
- to make the relative contribution of each difference to the error sum equal (by taking $w(i)=y_m(i)$);
- to convey the measurement error on each $y_m(i)$ to the minimization method.

Minimization of the least squares error constitutes a multidimensional nonlinear optimization problem. Several numerical methods for the approximate solution of such problems are available [2],[3]. They were originaly developed for use with analytical forward models; however, there is, in principle, no objection to the use of numerical models.

To find the minimization method best fitted to inverse semiconductor modelling, we implemented several methods and used them for doping profiling by inverse modelling (see below) [4]. The selection criteria were:

- the number of forward model evaluations needed for a certain degree of accuracy;
- the convergence span in parameter space.

It appeared that the Levenberg-Marquardt method [5], which is a blend between the classical methods of steepest descent and Newton's, requires the smallest number of model evaluations. An increased convergence span could be obtained with an improved version of this method, the Modified Damped Least Squares (MDLS) method [3]. In fig. 3, the optimization process is depicted in a 2-dimensional parameter space for the method of steepest descent and the MDLS method.

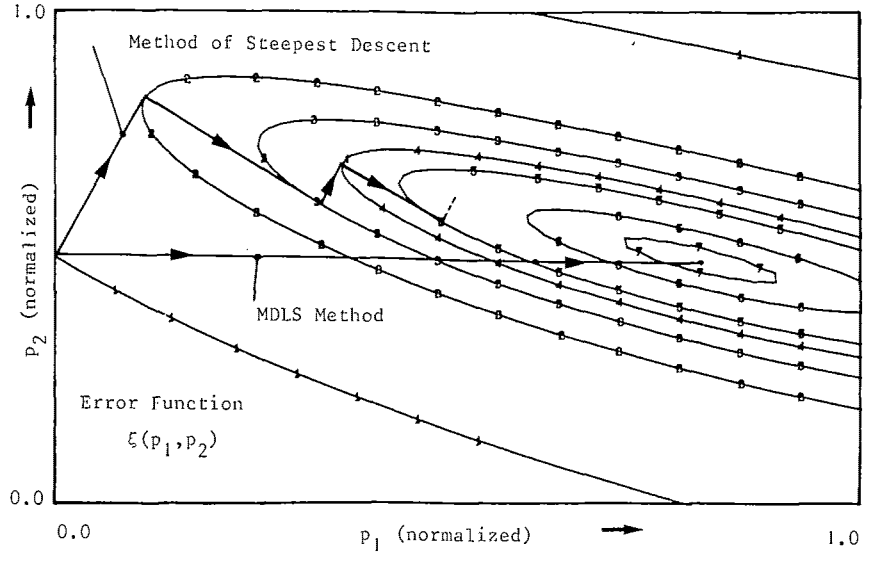

Fig 3. Minimization processes in a 2D parameter space

Almost all methods, including the MDLS method, use the derivatives of the measurement data with respect to the parameters in the minimization process. Usually, these are computed by forward differencing in the parameter space. This is a computationally expensive procedure, as in an N-dimensional parameter space N additional model evaluations are required. Therefore, it is very attractive when the forward model can internally generate these derivatives simultaneously with the model evaluation.

We implemented the MDLS method as a driver for inverse modelling as part of the general-purpose measurement data processing package, Profile [6]. This package provides I/O and graphical facilities, and also a choice of mathematical procedures such as expression evaluation, integration, differentiation, convolution, Fourier transform, curve-fit, etc. It can run interactively or as a programmed batch job. Profile may use internal forward models in the form of analytical expressions, but it may also communicate with external numerical models through data files and program calls.

3. EXAMPLE 1. DETERMINATION OF DOPING PROFILES

Conventionally, doping profiles are often determined by the Capacitance-Voltage (CV) method originated by Schottky [7]. The C(V) data are acquired from a reversed biased Schottky- or pn-diode, or from a MOS-structure. The doping profile N(x) is then computed by two parametric formulae:

$$N = \frac{C^3}{q\varepsilon \frac{dC}{dV}} \quad , \quad x = \frac{\varepsilon}{C} \quad . \tag{3.1}$$

These formulae have been derived using the abrupt depletion approximation, which assumes a sharp edge between the fully depleted and fully neutral regions of the device. Some disadvantages of the CV method are:

- the CV measurement data must be differentiated. For noisy measurements this may lead to considerable error;
- for steeply varying doping profiles the abrupt depletion approximation is not valid [8];
- the interpretation formulae are essentially 1-dimensional.

We used the method of inverse modelling to determine 1D doping profiles. To achieve this, we implemented a forward model in the form of the 1D poisson solver Fish [4], a program that computes C(V) data by solving Poisson's equation for a list of voltages, assembling a Q(V) profile and differentiating this to obtain a C(V) profile (note: C=dQ/dV). Care was taken to avoid significant discretisation error on C(V). Simulation of other electrical measurement data, such as channel conductance data [9] is also possible. For comparison purposes, both the abrupt depletion approximation and full Boltzmann statistics were implemented. In Fish, several analytical functions are available that describe the doping profile as a function of parameters

$$N(x) = f(x;\underline{p}). \tag{3.2}$$

As input data, the forward model Fish requires values for the doping parameter vector $\underline{p}$. The inverse modelling procedure then updates the parameter vector until a sufficiently small difference between measured and computed capacitances is obtained.

We applied this inverse poisson solver with good results to both real measurement data and synthetic measurement data used to validate the procedure. A result on synthetic data is shown in fig. 4. A synthetic C(V) profile was generated from a doping profile with an abrupt step (that could have been fabricated by Molecular Beam Epitaxy). The following function was used to model this doping profile in Fish:

$$\begin{aligned} N(x) &= N_{epi} \quad \text{if } x <= W_{step} \\ N(x) &= N_{step} \quad \text{if } x > W_{step} \end{aligned} \tag{3.3}$$

Hence, the three parameters N_{step}, N_{epi} and W_{step} were to be determined. Fig. 4a depicts three resultant profiles. The one by using inverse modelling with Boltzmann statistics exactly coincides with the original profile (a). The one with inverse modelling and the abrupt depletion approximation (b) shows a significant error. The conventional CV profile is not able to represent the sharpness of the doping edge (c). Fig. 4b shows the C(V) data for several iterations of the inverse model driver.

Fig. 4a. Original (a) and computed (a,b,c) doping profiles.

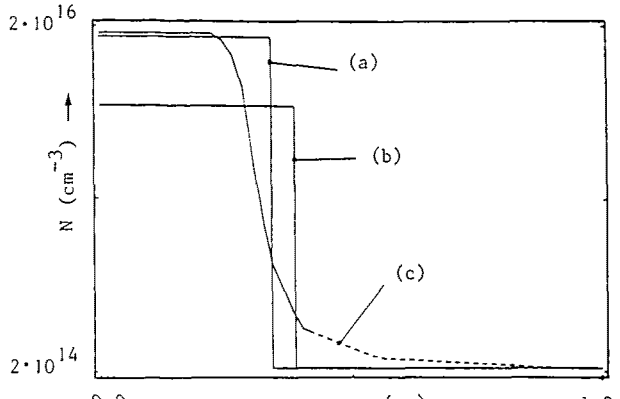

Fig. 4b. C(V) data for several iterations of the minimization procedure.

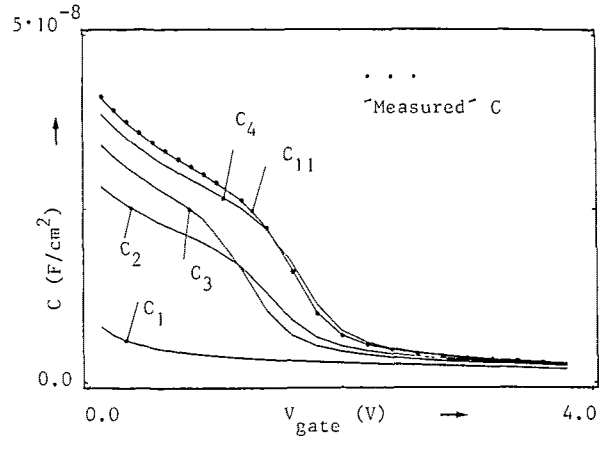

Fig. 4. Interpretation of CV data by inverse modelling

Currently, we are working on the extension of the inverse poisson solver in the 2-dimensional case (fig. 5). This calls for a 2D forward poisson solver and a 2D measurement device, from which capacitance data can be measured as a function of two independent voltages ($C(V_1,V_2)$). The doping profile must then be represented by an analytical function dependent on two spatial coordinates:

$$N(x,y) = f(x,y;\underline{p}). \qquad (3.4)$$

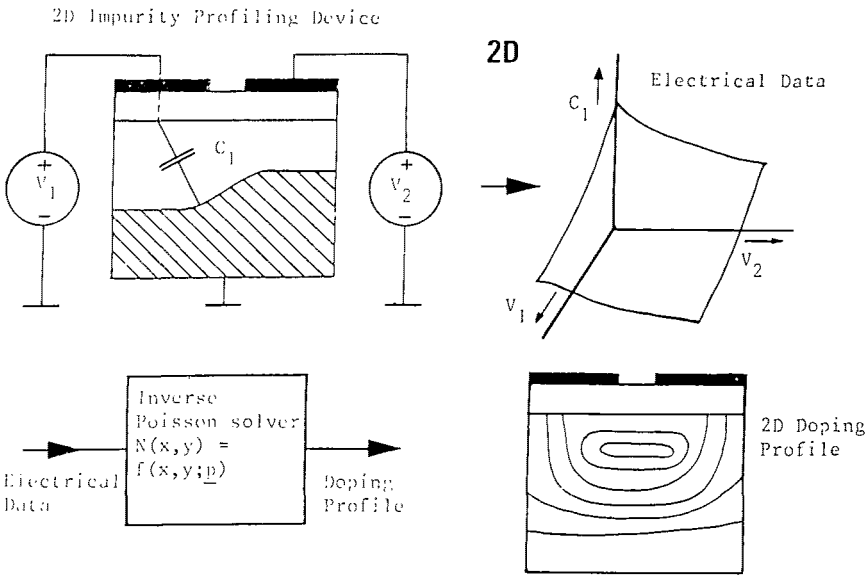

Fig. 5. Principle of 2D doping profiling by inverse modelling

4. EXAMPLE 2. EXTRACTION OF THE BUILT-IN ELECTRIC FIELD IN AN AMORPHOUS SILICON SOLAR CELL

Amorphous silicon solar cells consist of a p-i-n diode (fig. 6). The quality of such a solar cell depends strongly on the density of energy states in the undoped intrinsic layer. The density of states is, in its turn, reflected in the course of the built-in (zero-bias) electric field E(x). Therefore, it is desirable to determine the electric field experimentally. A suitable technique to do so is the time-of-flight method [10]. The device is excited by a short light pulse that generates a packet of excess electrons. It is assumed that the excess charge is small enough not to influence the field. Because of the field, the packet drifts through the device, thereby creating a current in the external measurement circuit which, in its

turn, results in a measurable voltage transient u(t). The current i(t) can be used to determine the electric field profile, if the drift mobility may be assumed to be constant.

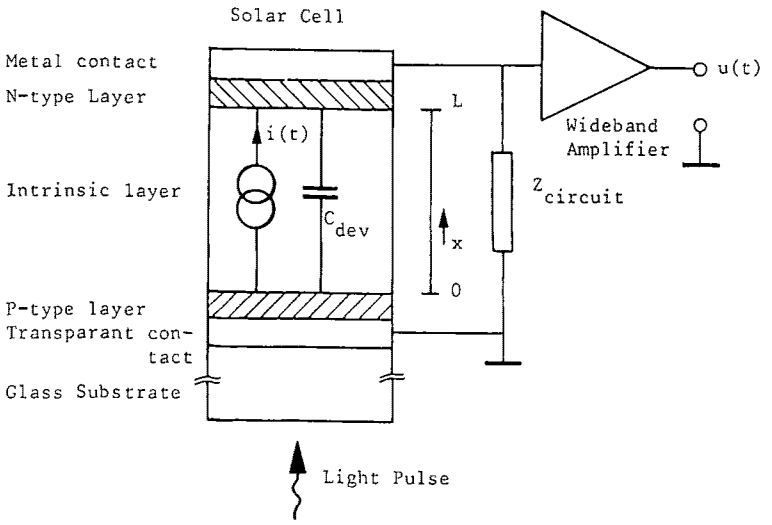

Fig. 6. Time-of-flight measurement on a solar cell

The movement of the excess charge through the device can be accurately modelled by the following transport equation

$$\frac{dn(x,t)}{dt} = -\frac{1}{q}\frac{dJ(x,t)}{dx} + f(t)g(x) - r(x)n(x,t) \qquad (4.1)$$

with $$J(x,t) = q\mu n(x,t)E(x) + qD\frac{dn(x,t)}{dx}\,. \qquad (4.2)$$

Here n is the electron concentration, E the (fixed) electric field, f describes the light pulse intensity as a function of time, g the carrier generation rate in the material as a function of place, and r describes the carrier recombination (lifetime). All other symbols have their usual meaning.

Previous workers were bothered by two main problems:
- the time resolution of the i(t) measurement was low due to the unknown disturbance caused by the measurement circuit;
- a grossly simplified model was used to find E(x) directly from measurements: f(t)g(x) combined into a Dirac pulse, no recombination r(x) and disregarding the diffusion term in (4.2).

Both problems were resolved by using a forward model of the entire setup including the measurement circuit [11]. The measured response u(t) can be computed using the simulated i(t) and the circuit pulse response H(t) by convolution:

$$u(t) = H(t)*i(t) \quad . \tag{4.3}$$

A wide bandwidth amplifier was used to ensure sufficient time resolution in the measured u(t).

Fig. 7a. Measured and simulated u(t) and i(t) transients.

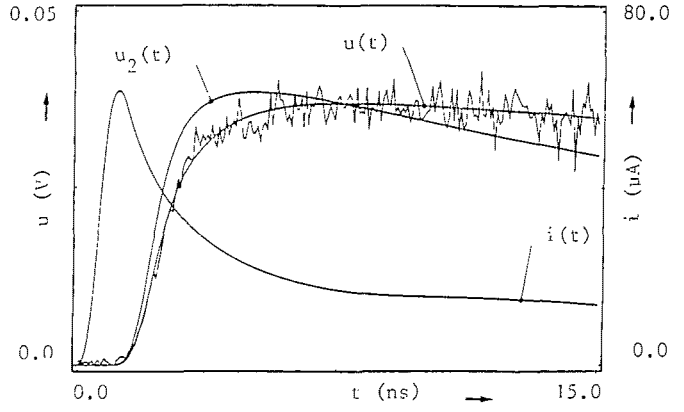

Fig. 7b. Extracted electric field profiles in an amorphous silicon solar cell.

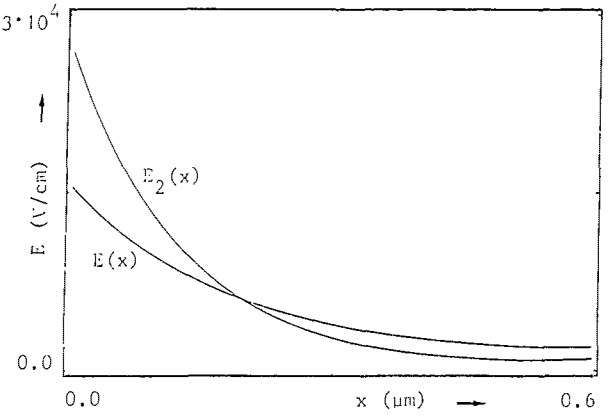

Fig. 7. Determination of the zero-bias electric field

The light pulse transient f(t) was measured and stored. The light excitation function was taken to be the usual exponential decay

$$g(x) = \alpha \exp(-\alpha x), \qquad (4.4)$$

with the value of α taken from literature [12]. The drift mobility μ was determined by carrying out a separate experiment. Accurate modelling of r(x) remained difficult; we assumed plausible values using a steady-state forward numerical model for amorphous silicon devices [14].
For the electric field, the following analytical model was used

$$E(x) = a_1 \exp(-b_1 x) + a_2 \exp(-b_2 x) + a_3 \exp(b_3 (L-x)) \qquad (4.5)$$

which is a logical extension of the single exponential function that can be derived if a constant density of states is assumed. Equations (4.1)-(4.2) are solved by forward differencing, applying the Lax-Wendroff scheme for the field term and the Crank-Nicholson method for the diffusion term [13].

The entire forward model is implemented as a Profile program [6], with a special-purpose routine for the solution of (4.1) and (4.2). As input variables this forward model requires the electric field parameters a_1 - b_3. Fig. 7 depicts the results of the inverse modelling on measured data. Fig. 7a shows the measured u(t) response of a 1.1 μm thick amorphous silicon solar cell (noisy line) and the final simulated u(t) response from the forward model. The corresponding simulated i(t) response is also depicted. In Fig. 7b the electric field profile corresponding to the modelled u(t) is shown. In fig. 7, $u_2(t)$ and $E_2(x)$ illustrate the sensitivity of the method by the simulation of a different excitation response and the corresponding field.

In the future, improvements on the inverse modelling of time-of-flight measurements on solar cells will be:
- the use of a more fundamental model that starts from a parametric expression for the density of states and computes both E(x) and the recombination rate r(x) from the density of states;
- more accurate charge-carrier transport modelling, for example, by Monte Carlo schemes instead of (4.1)-(4.2).

These improvements are easily within reach because the inverse modelling procedure can be applied to any feasible forward model.

5. CONCLUSION

Inverse modelling consists of the application of a nonlinear minimization method to a forward device model and measurement data. It allows the determination of physical parameters with-

out any restrictions imposed by the measurement interpretation method. For any physical effect that can be represented by a valid model, parameter values can be determined.

6. ACKNOWLEDGEMENTS

The authors wish to thank O.W. Memelink for the original idea of using a parametrized expression for doping profiling. Due recognition must also be paid to the authors of Numerical Recipes [13]. Many of the numerical routines they provided were flawlessly applied to our computations.

REFERENCES

[1] W. Crans and A.J. Berkhout, Assessment of seismic amplitude anomalies, Oil & Gas Jrnl, November 17, 1980, pp. 156-166.
[2] Y. Bard, Nonlinear Parameter Estimation, New York: Academic Press, 1974.
[3] M.A. Wolfe, Numerical Methods for Unconstrained Optimization, Wokingham: van Nostrand Reinhold, 1978.
[4] F. van Rijs, Master's Thesis (in Dutch), Delft University of Technology, November 1987.
[5] D.W. Marquardt, An Algorithm for Least Squares Estimation of non-linear Parameters, J. SIAM, Vol. 11, 1963, pp.431-441.
[6] G.J.L. Ouwerling, The Profile/Prof2d User's Manual, Delft University of Technology, October 1987.
[7] W. Schottky, Vereinfachte und erweiterte Theorie der Randschichtgleichrichter, Z. Phys., Vol. 118, pp. 539-592, 1942.
[8] D.P. Kennedy and R.R. O'Brien, On the measurement of impurity atoms by the differential capacitance technique, IBM J. Res. Dev., Vol. 13, 1969, p. 212.
[9] G.J.L. Ouwerling and M. Kleefstra, Monitoring the Impurity Profile and Thickness of Semiconductor Layers with the Channel Conductance of Buried Channel Field Effect Devices, Proc. ESSDERC 1987, North Holland, Amsterdam 1987, pp. 691-695.
[10] W.E. Spear, J. Non-Cryst. Solids, Vol. 1, 1969, p. 197.
[11] H.M. Wentinck, W. Stefan and J.W. Metselaar, Investigation of p-i interfaces by means of transient photoconductivity measurements, Proc. of the 8th European Photovoltaic Solar Energy Conference, Florence, May 1988, Reidel Publishing Co.
[12] J.I. Pankove (ed.), Semiconductors and Semimetals, Vol. 21: Hydrogenated Amorphous Silicon, Part B: Optical Properties, New York: Academic Press 1984.
[13] W.H. Press et al., Numerical Recipes, Cambridge: Cambridge University Press, 1986.
[14] H.M. Wentinck, Ph.D. Thesis (To be published), Delft University of Technology, 1988.